

Room-Temperature $\lambda \approx 2.7 \mu\text{m}$ Quantum Cascade Laser Sources Based on Intracavity Second-Harmonic Generation

Augustinas Vizbaras, *Student Member, IEEE*, Matthias Anders, Simeon Katz, Christian Grasse, *Student Member, IEEE*, Gerhard Boehm, Ralf Meyer, Mikhail A. Belkin, *Member, IEEE*, and Markus-Christian Amann, *Fellow, IEEE*

Abstract—We present experimental results on a short-wavelength quantum cascade laser based on intracavity second-harmonic generation. Our devices consist of an injectorless quantum cascade laser, which serves as a pump, and a transversely integrated passive two-well nonlinear section. The presented devices demonstrate above 1 mW output power at 2.65 μm emission wavelength with a record high peak conversion efficiency of 278 mW/W² at 80 K and still around 10 μW at 2.73 μm emission wavelength with 770 $\mu\text{W}/\text{W}^2$ conversion efficiency at room temperature. Experimental threshold current densities are demonstrated to be as low as 1.5 kA/cm² at room temperature.

Index Terms—III–V semiconductors, laser diodes, nonlinear mixing, quantum cascade lasers.

I. INTRODUCTION

SHORT-WAVELENGTH ($\lambda \leq 3.5 \mu\text{m}$) generation in quantum cascade lasers (QCLs) has been pursued by two different approaches: using materials with high conduction band offsets and intracavity second-harmonic (SH) generation. The first approach has led to the demonstration of highly-strained InGaAs/AlInAs/InP QCLs operating at 3.05 μm up to 105 K [1], InAs/AlSb QCLs emitting at 2.65 μm up to 175 K [2] and GaInAs/AlAsSb/InP QCLs emitting in the 3 μm –3.5 μm wavelength range up to room-temperature [3]. The threshold current density of these devices is getting higher with shorter wavelengths due to carrier scattering into indirect valleys of the well material [4]. An alternative approach to generate short-wavelength radiation from QCLs utilizes intracavity second-harmonic generation [5]–[10]. The advantage of this approach is that it is not directly affected by the carrier leakage into indirect valleys [11] of the conduction band,

Manuscript received November 22, 2010; revised January 13, 2011; accepted January 24, 2011. Date of current version April 1, 2011. This work was supported in part by the Excellence Cluster “Nanosystems Initiative Munich” and the Texas Higher Education Coordinating Board “Norman Hackerman Advanced Research Program” Award.

A. Vizbaras, M. Anders, C. Grasse, G. Boehm, R. Meyer, and M.-C. Amann are with the Walter Schottky Institut, Technische Universität München, München 85748, Germany (e-mail: augustinas.vizbaras@wsi.tum.de; matthias.anders@wsi.tum.de; grasse@wsi.tum.de; boehm@wsi.tum.de; ralf.meyer@wsi.tum.de; amann@wsi.tum.de).

S. Katz is with the Osram Opto-Semiconductors, Regensburg 93055, Germany (e-mail: simeon.katz@osram-os.com).

M. A. Belkin is with the Department of Computer and Electrical Engineering, University of Texas at Austin, Austin, TX 78758 USA (e-mail: mbelkin@ece.utexas.edu).

Color versions of one or more of the figures in this paper are available online at <http://ieeexplore.ieee.org>.

Digital Object Identifier 10.1109/JQE.2011.2109372

and could be realized in the conventional, well developed, InGaAs/AlInAs/InP material system for wavelength generation down to 2 μm . Additionally, nonlinear QCLs offer the possibility to achieve multi-frequency emission from the same chip, which could lead to tunable broad band sources in the entire 2 μm –10 μm wavelength range using the fundamental and second-harmonic signals of the laser. Numerous works have been reported on SH QCLs, however the device performance was limited to cryogenic temperatures due to high current densities of operation and limited conversion efficiency [5], [7], [8]. Recently, a novel approach, which uses transversely integrated passive nonlinear structures (NLs) has been suggested, and room-temperature operation of a SH QCL demonstrated [13]. In this paper, we present experimental results of a SH QCL based device with transversely integrated NL structure for wavelength emission around 2.7 μm . Our devices are based on a conventional strain-balanced AlInAs/GaInAs/InP material system. Quasi-phase-matching (QPM) technique [14] is used to compensate the wavevector mismatch between the fundamental and SH signal in our devices. We also use high-performance injectorless [15], [16] QCL active regions as our pumps in order to achieve low-current densities of operation. We demonstrate that SH output powers and conversion efficiencies can be improved by more than two orders of magnitude with a proper design.

II. DESIGN AND FABRICATION

A. Quantum Structure Design

In this work we used a $\lambda = 5.3 \mu\text{m}$ injectorless quantum cascade laser similar to the one in [15] as a pump. For SH generation, a two-well nonlinear structure has been designed consisting of two Ga_{0.35}In_{0.65}As quantum wells, separated by Al_{0.55}In_{0.45}As barrier (Fig.1). The structure was optimized to have the intersubband energy spacing resonant with the pump frequency. The nonlinear properties of such two-well nonlinear structure can be described using the quantum mechanics formalism as described in [17].

In the case when all electrons reside in the ground state, the expression for the second-order nonlinear susceptibility is given as (1):

$$\chi^{(2)} \approx \frac{e^3 N_1 z_{12} z_{23} z_{13}}{\hbar^2 \epsilon_0} \frac{1}{[(2\omega - \omega_{31}) + j\gamma_{31}][(\omega - \omega_{12}) + j\gamma_{12}]}. \quad (1)$$

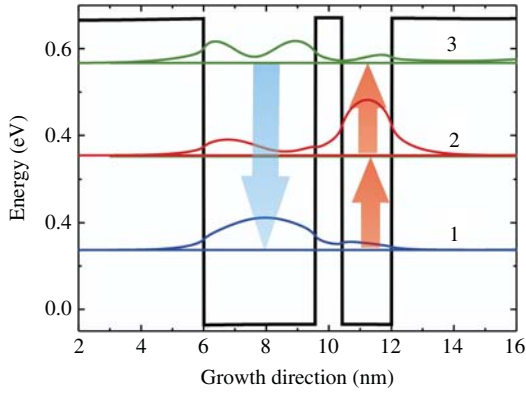


Fig. 1. Schematic conduction band structure of one period of the two-well nonlinear structure. The exact layer sequence (in nm) is: 6/3.57/0.85/1.59. Here the $\text{Al}_{0.55}\text{In}_{0.45}\text{As}$ barriers are shown in normal font, and the $\text{Ga}_{0.35}\text{In}_{0.65}\text{As}$ wells are in underlined font. The middle 2 nm of the 6 nm thick barrier are Si doped to $4 \times 10^{17} \text{cm}^{-3}$.

Here, e is the elementary charge, z_{ij} is the dipole matrix element between the states i and j , N_1 is the average carrier density in the ground state of the NL structure, \hbar is the Planck's constant, ϵ_0 is the vacuum permittivity, ω_{ij} is the frequency, corresponding to the transition between states i and j , and $2\gamma_{ij}$ is the full-width-half maximum (FWHM) of the transition between states i and j .

Assuming all fields being resonant with the intersubband transitions of the NL structure, and all transition linewidths equal to 16 meV, the nonlinear susceptibility value is calculated to be 1.7×10^4 pm/V. The dipole matrix elements for transitions between states 1-2, 2-3, and 3-1 are calculated to be 1.28 nm, 1.61 nm, and 0.44 nm respectively.

B. Device Design

The schematic longitudinal section of our device is presented in Fig 2. Our device consists of a 60 periods of injectorless QCL pump active region [15], designed to emit around $5.3 \mu\text{m}$, and followed by 55 periods of the NL section as shown in Fig. 1. The NL layer is structured into 50% duty cycle QPM grating in order to compensate for the inherent wavevector mismatch between the fundamental and the SH signals. In our case, the grating period was chosen to be around $37 \mu\text{m}$, which corresponds to a grating vector of 1700cm^{-1} . The passive NL section provides additional design flexibility, as it can be designed and patterned independently from the active region. Additionally, the simplicity of a two-well structure should have narrow transition linewidths, and the possibility of a separate doping reservoir allows higher doping levels in the NL section, while maintaining low doping levels in the pump active region for high performance. However, besides these advantages, passive NL structures also provide large resonant losses for the pump wave. These losses can be calculated using (2) [18]:

$$a_{res} \approx \frac{e^2 \omega z_{12}^2 n_{2D}}{\hbar \epsilon_0 n_{eff} c L_p} \frac{\gamma}{[(\omega - \omega_{12})^2 + \gamma^2]}. \quad (2)$$

Here e is the elementary charge, ω is the frequency of the pump signal, z_{12} is dipole matrix element for the transition

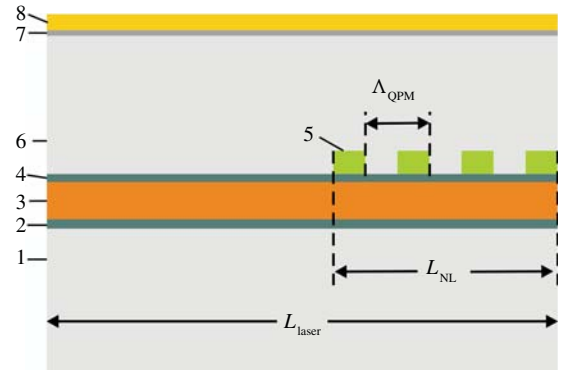


Fig. 2. Schematic of the longitudinal section of the SH-QCL used in this work. L_{NL} is the total length of the NL layer, L_{laser} is the total device length, Δ_{QPM} is the period of the QPM grating. Numbers indicate the following layers: 1-low-doped InP substrate, 2-lower GaInAs cladding, 3-active region of the pump, 4-upper GaInAs cladding, 5-two well NL structure, 6-low doped InP waveguide, 7-GaInAs top contact layer, 8-top metallization.

between states 1-2 in the NL structure shown in Fig. 1, n_{2D} is the sheet doping density in the NL structure, $2\gamma_{12}$ is the FWHM for the transition between states 1-2 in the NL structure shown in Fig. 1, \hbar is the Planck's constant, ϵ_0 is the vacuum permittivity, n_{eff} is the effective refractive index of the pump mode, c is the speed of light, and L_p is the NL period length. When the resonant losses are present, the threshold condition has to be modified in the following way:

$$j_{th} g_{th} \Gamma_{AR} = \alpha_i + \alpha_m + \frac{\Gamma_{NL} a_{res} F}{2}. \quad (3)$$

Here, j_{th} is the threshold current density, g_{th} is the threshold gain coefficient, Γ_{AR} is mode confinement factor in the pump active region, α_i is the intrinsic modal loss value, α_m is the mirror loss, Γ_{NL} is the mode confinement factor in the NL layer, a_{res} is the resonant loss value, F is the NL filling factor, and is equal to L_{NL}/L_{Laser} . The factor of 2 in the denominator of the third term comes from the fact that we use a 50 % duty cycle QPM grating.

From mode simulations, we estimated the confinement factor in the NL layer to be around 13%, which leads to the resonant modal loss value around 58cm^{-1} for the pump signal. Such high additional losses will strongly affect the performance of the pump, therefore the length of the NL grating has to be modified. Additionally, we use injectorless QCL active regions as pumps due to their high gain [19], and low threshold performance.

C. Device Growth and Fabrication

The growth of the device structure, presented in this letter was done collectively by MBE and MOVPE. First, the 60 repetitions of the injectorless QCL pump active region, followed by 55 repetitions of the NL structure were grown by MBE. Then the sample was taken out of the growth chamber, and the top NL layer was structured into QPM gratings of different length by optical lithography and selective wet-chemical etching. Afterwards, the sample was cleaned in a buffered HF solution and transferred into MOVPE chamber, where the top $4 \mu\text{m}$ of InP waveguide, doped to $4 \times 10^{16} \text{cm}^{-3}$, followed by 200 nm

of n^+ InP plasmon layer, doped to $5 \times 10^{18} \text{cm}^{-3}$ and 50 nm of n^{++} GaInAs contact layer were overgrown. After the epitaxial steps, the sample was processed into conventional deep-etched ridge waveguide lasers by combination of optical lithography, dry-etching, dielectric sputtering, PECVD, e-beam evaporation of metals. For characterization, the lasers had a SiN/Ti/Au high-reflectivity (HR) facet coating on their back facet, whereas the front facet was coated with ~ 300 nm SiN, which served as a dichroic coating, providing around 19 % reflectivity for the fundamental wave, and around 2 % for the SH wave. For characterization, the sample was cleaved into laser bars of different length, which were mounted on Cu heatsinks epi-side up.

III. SH POWER AND CONVERSION EFFICIENCY

The power of the SH signal is given by (4) [17]:

$$W_2 = \frac{\omega_1^2}{2n_1^2 n_2 \epsilon_0 c^3} \left| \frac{\chi^{(2)}}{\pi} \right|^2 \frac{W_1^2}{S_{eff}} l_{eff}^2. \quad (4)$$

Here $W_{1,2}$ are the fundamental and SH powers, $n_{1,2}$ are the effective refractive indices for the fundamental and SH modes, c is the speed of light, ϵ_0 is the vacuum permittivity, S_{eff} is the effective area of interaction and is given in (5), l_{eff} is the effective length of interaction given by (6), and $\chi^{(2)}$ is the second-order nonlinear susceptibility, given by (1).

The effective area of interaction characterizes the modal overlap between the two waves, and can be obtained from the simulated mode profiles (5):

$$S_{eff} = \frac{|\chi^{(2)}|^2 \int (H_{2\omega}(x, z))^2 dx dz \left(\int H_{\omega}(x, z)^2 dx dz \right)^2}{\left| \int_{NL} H_{2\omega}(x, z) (H_{\omega}(x, z))^2 \chi^{(2)} dx dz \right|^2}. \quad (5)$$

Here, $H_{\omega, 2\omega}$ are the amplitudes of the fundamental and the SH waves, z is the growth direction, and x is the direction perpendicular to the growth, and the propagation directions. In our calculations we assumed $\chi^{(2)}$ to be constant in the NL section and equal to 0 elsewhere. The numerator of (5) is integrated over the entire structure, whereas the denominator is integrated over the NL section only [5, 7, 13]. Assuming the ridge width of $12 \mu\text{m}$, the effective area of interaction was calculated to be $5288 \mu\text{m}^2$ for our devices. This factor is higher than for integrated NL designs [5, 7, 8, 12], but we hope to compensate it with a higher $\chi^{(2)}$ value provided with our passive NL structure.

Another important parameter is the so-called effective length of interaction l_{eff} , which is a function of the modal loss for the two waves and the wavevector mismatch between them. The exact solution can be obtained by solving the coupled wave equations for the fundamental and SH waves. The final expression yields (6):

$$l_{eff} = \sqrt{\frac{e^{-\alpha_2 L} \left(e^{-\Delta k L} e^{-(\alpha_1 - \frac{\alpha_2}{2})L} - 1 \right)^2}{(\alpha_1 - \frac{\alpha_2}{2})^2 + \Delta k^2}}. \quad (6)$$

Here, $\alpha_{1,2}$ are the total modal losses for the fundamental and SH signals, L is the length of the NL grating, and Δk is the wavevector mismatch between the waves.

It is often helpful to evaluate the so-called conversion efficiency, which is a commonly used figure of merit (FOM) of nonlinear devices. The internal conversion efficiency is given as (7):

$$\eta_{int} = \frac{W_2}{W_1^2}. \quad (7)$$

However, what we experimentally measure is the external conversion efficiency, which depends of the mirror reflectivities, and the total modal loss in the NL section. The expression for the external conversion efficiency is given by (8):

$$\eta_{ext} = \eta_{int} \frac{1 - R_2}{(1 - R_1)^2} e^{2\alpha_{\omega}^* L}. \quad (8)$$

Here, $R_{1,2}$ are the power reflectivities of the facet for the fundamental and SH waves, L is the length of the NL grating, and $\alpha_{\omega}^* = (\Gamma_{NL} \alpha_{res}/2) - g_{th} \Gamma_{AR}$ is the net modal intensity loss for the fundamental light in the nonlinear section, and $g_{th} \Gamma_{AR}$ is the modal gain as given by (3).

IV. EXPERIMENTAL RESULTS AND DISCUSSION

A. Calibrated Power and Spectral Measurements

Devices, presented in this letter were measured in pulsed mode. For calibrated SH power measurements, a HgCdTe detector, calibrated with a thermopile was used. The detector was equipped with two short-wave pass filters with a total attenuation of 70 dB above $3.4 \mu\text{m}$. For power measurements the devices were driven with 500 ns long pulses at a repetition rate of 10 kHz.

Spectral measurements were performed using a FTIR spectrometer V70 from Bruker. Spectra were recorded with 1cm^{-1} resolution in rapid scan mode using room-temperature detector RT-DLaTGS for 80 K measurements, and a liquid nitrogen cooled InSb detector was used for RT SH spectral measurements. During all measurements the detectors were equipped with short-wave pass filters to avoid any influence of the fundamental signal. For spectral measurements, the devices were driven with 800 ns long pulses at a repetition rate of 8.3 kHz.

B. $T = 80 \text{K}$ Results

For characterization, device with different NL grating lengths were fabricated. At first, it was interesting to see the effect of resonant losses. Fig. 3 shows the light intensity – threshold current density ($L - j$) data for two 4 mm long and $12 \mu\text{m}$ wide devices from the same chip. The laser A has the entire NL grating removed prior the MOVPE overgrowth, whereas the laser B has a 50 % duty cycle QPM grating over the entire length of the mesa. In order to evaluate resonant losses, we have to write the threshold condition for both lasers, and solve the following system of equations:

$$\begin{cases} j_{thA} = \frac{\alpha_i + \alpha_m}{g_{th} \Gamma_{AR}}, \\ j_{thB} = \frac{\alpha_i + \alpha_m + \frac{\Gamma_{NL} \alpha_{res}}{2}}{g_{th} \Gamma_{AR}}. \end{cases} \quad (9)$$

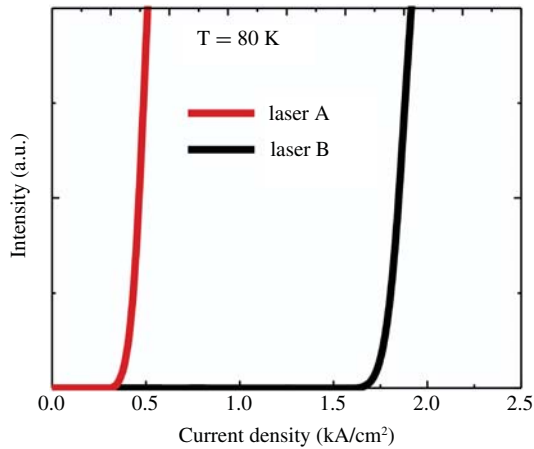


Fig. 3. Effect of the resonant loss. Sample A has no NL grating, thus no resonant losses, whereas sample B has a 4 mm long NL grating. Both lasers are on the same chip, 4 mm long and 12 μm wide. Both facets are left uncoated.

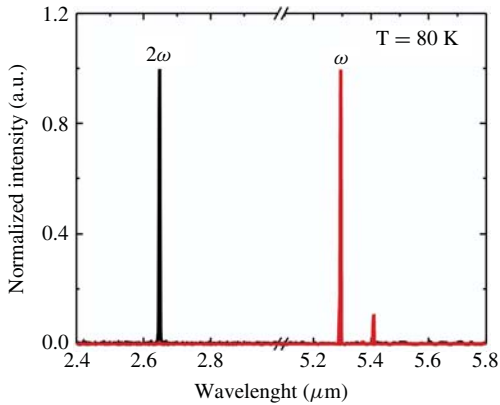


Fig. 4. 80 K emission spectra for the 3.5 mm long and 12 μm wide device with a 1 mm long NL grating at a current density of around 1.8 kA/cm^2 . The device had a HR coating on the back facet and a dichroic coating on the front facet, as has been explained in the main text.

Using the experimental threshold current density values from Fig. 3, we can extract the total modal resonant loss value of 50.24 cm^{-1} . This value is in fair agreement with the estimated value of 58 cm^{-1} , and could imply that our pump frequency is close to resonance, detuned from the NL resonance only by a few meV.

The presence of such very high resonant losses clearly reduces the performance of the pump, therefore, shorter NL gratings were used. At 80 K, the best performing device had a 1 mm long NL grating. Fig. 4 shows the emission spectra for both fundamental and SH signals. The SH signal has a peak wavelength around 2.65 μm , which is the shortest wavelength for any InP-based intersubband device reported so far [1], [3], [13]. This clearly indicates that intracavity nonlinear mixing can dramatically extend the emission spectrum of conventional InP QCLs.

Calibrated power results for the same device are presented in Fig. 5. It can be seen that our best performing device was able to deliver above 1 mW of peak pulsed output power. The peak external conversion efficiency is $278 \text{ mW}/\text{W}^2$. The latter value is around two orders of magnitude higher than for any

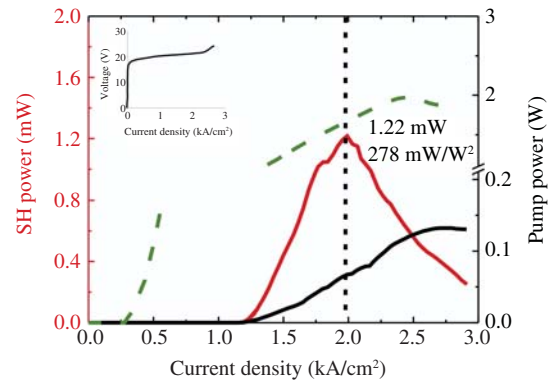


Fig. 5. Calibrated L - j data for the fundamental (black line) and SH (red line) signals at 80 K. The vertical dashed line indicates the point where peak conversion efficiency is calculated. The green dashed line indicates the L - j curve for a laser without the NL grating. The inset shows the V - j data for the same laser.

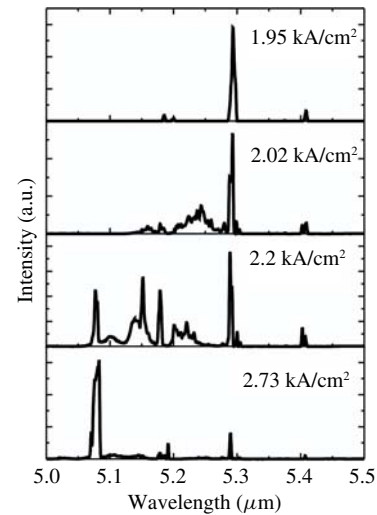


Fig. 6. Spectral evolution of the pump signal with increasing current density at 80 K. The intensity is normalized for better view.

nonlinear QCL-based device reported so far [5], [7], [8], [9], [12], [13].

In fact, if we assume 3 meV detuning from resonance, which would correspond to the measured modal resonant loss, the estimated external conversion efficiency value is $307 \text{ mW}/\text{W}^2$ and is in a very good agreement with the experimental value. As can be seen from Fig. 5, the power dependence of the SH signal does not follow the expected quadratic behavior. We believe that this is due to several factors: first, the frequency shift of the pump signal with increasing current, which affects our nonlinear properties, which have a strong frequency dependence as can be seen from (1), second, the multimode nature of our Fabry-Perot devices, and third the power saturation effects which, due to the small dimensions of our devices, cannot be neglected. In fact, by using the calculated mode profiles, and the calculated dipole matrix elements we estimate the saturation power value around 80 mW, which implies that this effect should be present in our devices. The effect of the resonant loss in the NL section is clearly visible from the comparison of the L - j curves of the lasers with and without the NL grating (Fig. 5). In addition to impressive output

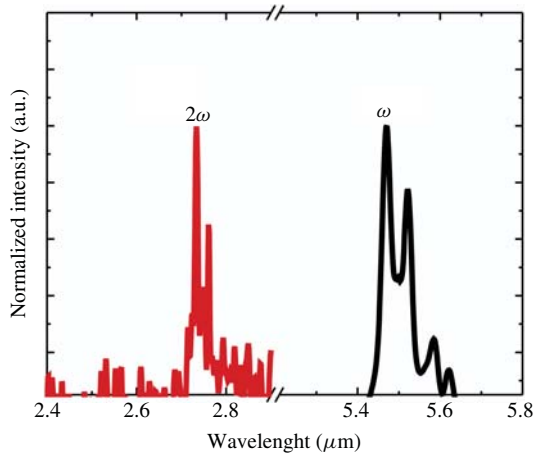


Fig. 7. Room-temperature emission spectrum of a 5 mm long and 12 μm wide laser with 200 μm long NL grating. The measured device had a HR coating on the back facet and a dichroic coating on the front facet.

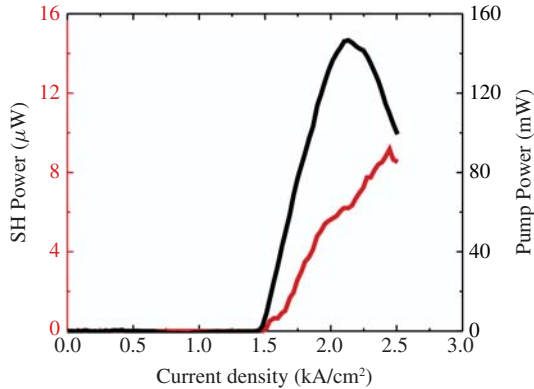


Fig. 8. Room-temperature L - j data for a 5 mm long and 12 μm wide laser with 200 μm long NL grating. The measured device had a HR coating on the back facet and a dichroic coating on the front facet.

performance, the operating current densities are kept relatively low, which could be important for future developments of SH QCLs operating in continuous-wave. It can be seen from Fig. 5 that the SH signal reaches roll-over before the pump signal does. This behavior is attributed to the appearance of higher order transversal modes, and the strong wavelength shift of the pump signal with increasing current due to the Stark effect (Fig. 6). Such spectral behavior is an inherent property of our pump laser, and does not depend on the fact whether the NL section is present or not.

C. Room-Temperature Operation

Devices with 1 mm long NL grating were not suitable for room-temperature operation due to the early onset of the negative differential resistance (NDR) (inset in Fig. 5), as the threshold has been heavily affected by the additional resonant loss in the NL section (Fig. 3 and 5). Therefore, in order to minimize the effect of the resonant loss, the NL grating had to be further shortened. We found that devices with 200 μm long NL gratings were able to operate at room-temperature. The emission spectrum, of the 5 mm long device with a 200 μm NL grating is shown in Fig. 7. It can be seen that the emission wavelength is slightly red-shifted, with a peak around

2.73 μm . The RT L - j data is presented in Fig. 8. The peak pulsed output power was measured to be around 9 μW with a peak external conversion efficiency around 0.77 mW/W^2 . Even though these values are lower compared to 80 K, they still represent the highest values for SH QCLs reported to date. We believe, that at RT, the frequency of the pump is red-shifted from the resonance of the NL. This can be seen from the L - j data for the fundamental and SH signals in Fig. 8. Here, even though the pump signal reaches roll-over, the power of the SH signal increases further. This can be explained by the blue-shift of the emission frequency of the pump signal with increasing current. At a certain point, the increase of the nonlinear properties of the NL section overcompensate the drop of the pump power, and the SH signal increases further.

Finally, the operating current densities for our devices are much lower than for any other SH QCL device reported to date. We attribute this to the excellent performance of our injectorless pump active region.

V. CONCLUSION

In conclusion, we have demonstrated that it is possible to extend the wavelength of InP-based QCLs to very short-wavelengths by intracavity second-harmonic generation, using the conventional AlInAs/GaInAs/InP material system. Moreover we have demonstrated that decent power levels can be obtained with very high conversion efficiencies. Such approach could lead to the realization of a very compact, broadband source with a spectral coverage in the whole wavelength range between 2 μm and 8 μm by combining the fundamental and nonlinear signals in a single heterogeneous active region based QCL device.

REFERENCES

- [1] M. P. Semtsiv, M. Wienold, S. Dressler, and T. Masselink, "Short-wavelength ($\lambda \approx 3.05 \mu\text{m}$) InP-based strain-compensated quantum-cascade laser," *Appl. Phys. Lett.*, vol. 90, no. 5, pp. 051111-1–051111-3, Jan. 2007.
- [2] O. Cathabard, R. Teissier, J. Devenson, J. C. Moreno, and A. N. Baranov, "Quantum cascade lasers emitting near 2.6 μm ," *Appl. Phys. Lett.*, vol. 96, no. 14, pp. 141110-1–141110-3, Apr. 2010.
- [3] S. Y. Zhang, D. G. Revin, J. W. Cockburn, K. Kennedy, A. B. Krysa, and M. Hopkinson, " $\lambda \sim 3.1 \mu\text{m}$ room temperature InGaAs/AlAsSb/InP quantum cascade lasers," *Appl. Phys. Lett.*, vol. 94, no. 3, pp. 031106-1–031106-3, Jan. 2009.
- [4] M. P. Semtsiv, M. Wienold, S. Dressler, W. T. Masselink, G. Fedorov, and D. Smirnov, "Intervalley carrier transfer in short-wavelength InP-based quantum-cascade laser," *Appl. Phys. Lett.*, vol. 93, no. 7, pp. 071109-1–071109-3, Aug. 2008.
- [5] N. Owschimikow, C. Gmachl, A. Belyanin, V. Kocharovskiy, D. L. Sivco, R. Colombelli, F. Capasso, and A. Y. Cho, "Resonant second-order nonlinear optical processes in quantum cascade lasers," *Phys. Rev. Lett.*, vol. 90, no. 4, pp. 043902-1–043902-4, Jan. 2003.
- [6] I. Vurgaftman, J. R. Meyer, and L. R. Ram-Mohan, "Optimized second-harmonic generation in asymmetric double quantum wells," *IEEE J. Quantum Electron.*, vol. 32, no. 8, pp. 1334–1346, Aug. 1996.
- [7] C. Gmachl, A. Belyanin, D. L. Sivco, M. L. Peabody, N. Owschimikow, A. M. Seargent, F. Capasso, and A. Y. Cho, "Optimized second-harmonic generation in quantum cascade lasers," *IEEE J. Quantum Electron.*, vol. 39, no. 11, pp. 1345–1355, Nov. 2003.
- [8] M. Giovannini, M. Beck, N. Hoyler, and J. Faist, "Second harmonic generation in (111)-oriented InP-based quantum cascade laser," *J. Appl. Phys.*, vol. 101, no. 10, pp. 103107-1–103107-4, May 2007.

- [9] M. A. Belkin, M. Troccoli, L. Diehl, F. Capasso, A. A. Belyanin, D. L. Sivco, and A. Y. Cho, "Quasi-phase matching of second-harmonic generation in quantum cascade lasers by Stark shift of electronic resonances," *Appl. Phys. Lett.*, vol. 88, no. 20, pp. 201108-1–201108-3, May 2006.
- [10] M. M. Fejer, S. J. B. Yoo, R. L. Byer, A. Harwit, and J. S. Harris, Jr., "Observation of extremely large quadratic susceptibility at 9.6–10.8 μm in electric-field-biased AlGaAs quantum wells," *Phys. Rev. Lett.*, vol. 62, no. 9, pp. 1041–1044, Feb. 1989.
- [11] Y.-H. Cho and A. Belyanin, "Short-wavelength infrared second harmonic generation in quantum cascade lasers," *J. Appl. Phys.*, vol. 107, no. 5, pp. 053116-1–053116-7, Mar. 2010.
- [12] O. Malis, A. Belyanin, C. Gmachl, D. L. Sivco, M. L. Peabody, A. M. Seargent, and A. Y. Cho, "Improvement of second-harmonic generation in quantum-cascade lasers with true phase matching," *Appl. Phys. Lett.*, vol. 84, no. 15, pp. 2721–2723, Apr. 2004.
- [13] M. Jang, R. W. Adams, J. X. Chen, W. O. Charles, C. Gmachl, L. W. Cheng, F.-S. Choa, and M. A. Belkin, "Room-temperature operation of 3.6 μm In_{0.53}Ga_{0.47}As/Al_{0.48}In_{0.52}As quantum cascade laser sources based on intracavity second harmonic generation," *Appl. Phys. Lett.*, vol. 97, no. 14, pp. 141103-1–141103-3, 2010.
- [14] M. M. Fejer, G. A. Magel, D. H. Jundt, and R. L. Byer, "Quasi-phase-matched second harmonic generation: Tuning and tolerances," *IEEE J. Quantum Electron.*, vol. 28, no. 11, pp. 2631–2654, Nov. 1992.
- [15] S. Katz, A. Vizbaras, G. Boehm, and M.-C. Amann, "High-performance injectorless quantum cascade lasers emitting below 6 μm ," *Appl. Phys. Lett.*, vol. 94, no. 15, pp. 151106-1–151106-2, Apr. 2009.
- [16] S. Katz, G. Boehm, and M.-C. Amann, "Low-threshold injectorless quantum cascade laser with four material compositions," *Electron. Lett.*, vol. 44, no. 9, pp. 580–581, 2008.
- [17] R. W. Boyd, *Nonlinear Optics*, 3rd ed. New York: Academic, 2008, pp. 69–204.
- [18] R. Paiella, *Intersubband Transitions in Quantum Structures*, 1st ed. New York: McGraw-Hill, 2006, pp. 1–41.
- [19] S. Katz, A. Vizbaras, G. Boehm, and M.-C. Amann, "Nonlinear gain behavior in injectorless quantum cascade lasers," *Opt. Eng.*, vol. 49, no. 11, p. 111107, Nov. 2010.



Augustinas Vizbaras (S'09) was born in Panevezys, Lithuania, in 1984. He received the B.Sc. degree in electronics engineering from Vilnius University, Vilnius, Lithuania, in 2007, and the M.Sc. degree in physics from the Royal Institute of Technology, Stockholm, Sweden, in 2009. He is currently pursuing the Ph.D. degree at the Walter Schottky Institut, Technische Universität München, Munich, Germany.

He has authored or co-authored 15 research papers on semiconductor lasers and detectors in scientific

journals and conference proceedings. His current research interests include development of terahertz and mid-IR quantum cascade lasers, including device design, fabrication, and characterization.

Mr. Vizbaras is a Graduate Student Member of the Society of Photo-Optical Instrumentation Engineers and the IEEE Photonics Society.



Matthias Anders was born in Dachau, Germany, in 1984. He received the Diploma degree in engineering physics from the Technische Universität München, Munich, Germany, in 2005. His main subjects were semiconductor physics and renewable energies. He received the Diploma degree on the basis of a thesis on short-wavelength quantum cascade lasers at the Walter Schottky Institut, Technische Universität München, in December 2010.



Simeon Katz received the B.E. degree in electrical engineering from the Technische Universität München, Munich, Germany, the Diploma degree in 2007, and the Honors degree in technology management from the Bavarian Elite Network, Munich, in 2006.

He is currently working for Osram Opto-Semiconductors, Regensburg, Germany, in the field of device and material analytics. He has authored or co-authored more than 20 (including four invited) papers on quantum cascade lasers in scientific journals and conference proceedings during his Ph.D. degree.



Christian Grasse (S'09) was born in Munich, Germany, in 1981. He received the Diploma degree in physics from Technische Universität München, Munich, in 2007. He is currently pursuing the Ph.D. degree at the Walter Schottky Institut, Technische Universität München.

He has authored or co-authored 14 papers on semiconductor materials and devices in scientific journals and conference proceedings. His current research interests include metal-organic vapor phase epitaxy growth of III–V compounds for long-wavelength

lasers.

Mr. Grasse is a Graduate Student Member of the IEEE Photonics Society.



Gerhard Boehm received the Technical Physics degree from the Fachhochschule Muenchen, Munich, Germany, and the Diploma degree in 1988.

He is now with the Walter Schottky Institute, Technische Universität München, Munich. His current research interests include epitaxial growth of III–V semiconductor structures, quantum cascade lasers, and long-wavelength vertical-cavity and edge-emitting laser-diodes.



Ralf Meyer was born in Oldenburg, Germany, in 1963. He received the Diploma degree in physics from the Rheinisch-Westfälische Technische Hochschule Aachen, Aachen, Germany, for his work on metal-organic vapour phase epitaxy growth of GaInAsP/InP heterostructures for laser applications, in 1990. He received the Ph.D. degree from the Research Center Jülich, Jülich, Germany, in 1994. While composing his Ph.D. thesis, he developed the heterostructures based on GaInAs and InP for basic research on transport properties in low-dimensional systems and the fabrication of high-speed transistors.

He was with the Department of Electrical Engineering, University of Kassel, Kassel, Germany, where he collaborated in establishing a research group and took a leading position in the founding of the Institute for Microstructure Technology and Analytics, Karlsruhe, Germany. He became a Head of the III–V Technology Group at the Walter Schottky Institut, Technische Universität München, Munich, Germany, in 1998, which is dedicated to the development and realization of a variety of different types of light emitters in the wavelength range from 1 to 10 μm based on III–V compound semiconductors. He has collaborated on several national and European projects. In the framework of the latter, he fabricated InP-based buried heterostructures by means of metal-organic vapor phase epitaxy to realize electrically widely tuneable distributed feedback lasers for telecom applications. He has authored or co-authored some 60 papers in the field of fabrication of heterostructures for basic research as well as electronic and optoelectronic devices based on III–V compound semiconductors. In 2003, he organized the German Workshop on Molecular Beam Epitaxy.

Dr. Meyer is a member of the German Physical Society.



Mikhail A. Belkin (M'07) received the B.S. degree in physics and mathematics from the Moscow Institute of Physics and Technology, Moscow, Russia, in 1998, and the Ph.D. in physics from the University of California, Berkeley, in 2004.

He is an Assistant Professor in the Department of Electrical and Computer Engineering, University of Texas at Austin, Austin. From 2004 to 2008, he was with the School of Engineering and Applied Sciences, Harvard University, Cambridge, MA, first as a Post-Doctoral Fellow from 2004 to 2006, and then as a Research Associate from 2006 to 2008. He joined the Department of Electrical and Computer Engineering, University of Texas at Austin, in 2008. His current research interests include development of mid-infrared and terahertz quantum cascade lasers with novel functionalities, mid-infrared spectroscopy and microscopy at the nanoscale, and plasmonic devices and metamaterials.



Markus-Christian Amann (SM'91–F'07) was born in Singen/Hohentwiel, Germany, in 1950. He received the Diploma degree in electrical engineering and the Dr.Ing. degree from the Technische Universität München, Munich, Germany, in 1976 and 1981, respectively. During his thesis work, he studied superluminescent diodes and low-threshold laser diodes and developed the AlGaAs-GaAs metal-clad ridge-waveguide laser.

He was with the Corporate Research Laboratories of Siemens AG, Munich, from 1981 to 1994, where he was involved in the research on long-wavelength InGaAsP-InP laser diodes. In 1990, he became a Deputy Director of Research on laser diodes and integrated optoelectronic devices. In February 1994, he joined the Department of Electrical Engineering, University of Kassel, Kassel, Germany, as a Full Professor for Technical Electronics, establishing a working group for III–V semiconductor electronics and optoelectronics. Since November 1997, he has held the Chair of Semiconductor Technology at the Walter Schottky Institute, Technical University of Munich, where he is currently engaged in research on tunable laser diodes for near-infrared, quantum cascade lasers, long-wavelength vertical-cavity laser-diodes, and laser diode applications. He has authored or co-authored some 400 research papers on semiconductor optoelectronics in scientific journals and conference proceedings, has given several talks (including some 50 invited) and co-authored two books on these subjects.

Dr. Amann is a member of the German Information Technische Gesellschaft, and a Fellow of the IEEE Lasers and Electro-Optics Society. He has served on numerous conference committees such as the IEEE Semiconductor Laser Conferences, the Indium Phosphide and Related Materials Conferences, and the Conferences on Lasers and Electro-Optics.